Supplement of Atmos. Chem. Phys., 23, 4343–4359, 2023
https://doi.org/10.5194/acp-23-4343-2023-supplement

Atmospheric Chemistry and Physics
Open Access

Supplement of

High frequency of new particle formation events driven by summer monsoon in the central Tibetan Plateau, China

Lizi Tang et al.

Correspondence to: Min Hu (minhu@pku.edu.cn)

List of the supporting information:

Section S1. The representativeness of the observation periods

Section S2. Details about model simulations

Table S1. Model performance of meteorological factors at Nam Co station

Table S2. Model performance of air pollutants at Nam Co station

Figure S1. The Indian Summer Monsoon (ISM) Index in 2019

Figure S2. WRF/CMAQ modeling domain

Figure S3. Comparison of simulated and observed wind direction and wind speed

Figure S4. Comparison of simulated and observed RH and temperature

Figure S5. Comparison of simulated and observed PM, O_3 and VOC

Figure S6. Comparison of simulated and observed SO_2 at Mt. Yulong.

Figure S7. Relationship between SO_2 and BC at Mt. Yulong in 2015

Figure S8. Relationship between modelled SO_2 and BC at Nam Co station

Figure S9. Typical particle number size distributions of a NPF day, an undefined day and non-event day

Figure S10. Comparison in frequency distributions of temperature, RH, H_2O and WS in pre-monsoon and monsoon seasons

Figure S11. Wind rose plots in pre-monsoon and monsoon seasons

Figure S12. The frequencies of the 48 h back trajectories of air masses in pre-monsoon and monsoon seasons

Figure S13. Comparison in frequency distributions of $PM_{0.8}$, BC, O_3 and CO in pre-monsoon and monsoon seasons

Figure S14. Model spatial distribution of SO_2 in non-event days, NPF-pre days and NPF-monsoon days

Figure S15. Diurnal variations of the concentration of toluene, styrene and trimethylbenzene in NPF-pre days and non-event days.

Figure S16. Wind rose plots in non-event days, NPF-pre days and NPF-monsoon days

Figure S17. Model spatial distribution of wind field in non-event days, NPF-pre days and NPF-monsoon days

Figure S18. Determination of the aerosol production in 17 June, 2019

Section S1 The representativeness of the observation periods

The measurement was conducted from 26 April to 22 May, 2019 and 15 June to 25 June, 2019, and can be representative of the pre-monsoon season and monsoon season, respectively.

Firstly, the intensity of Indian Summer Monsoon during the two measurements periods can represent that in the whole pre-monsoon and monsoon seasons, respectively. The intensity of Indian Summer Monsoon is an important indicator to distinguish the monsoon season. Here the intensity of Indian Summer Monsoon (ISM) was indicated by the ISM Index, which are defined by the negative outgoing longwave radiation anomalies (with respect to the climatological annual cycle) averaged over the Bay of Bengal–India region (10°–25°N, 70°–100°E) (Wang and Fan, 1999). As shown in Fig. S1, the measurement periods (green boxes) were in the pre-monsoon season (March-May) and monsoon season (June-September), respectively. And the IMS index during the two measurements periods were equivalent to those of the whole pre-monsoon season (average: -19.5 vs -20.7 W m^{-2}) and monsoon season (average: 27.0 vs 26.3 W m^{-2}), respectively.

Secondary, the characteristics of meteorology and atmospheric pollutants in the two measurements periods was generally in agreement with the previous long-term studies at Nam Co station and other sites in the Tibetan Plateau (TP) (Yin et al., 2017; Cong et al., 2015; Bonasoni et al., 2010; Xu et al., 2018). That is, the characteristics of meteorology (temperature, WS and RH) and atmospheric pollutants (PM, BC and ozone) in the two measurements periods were matched with those in the whole pre-monsoon and monsoon season at Nam Co station and other sites in the TP.

Therefore, the two observation periods are representative in the seasonal characteristics in pre-monsoon season and monsoon season, respectively.

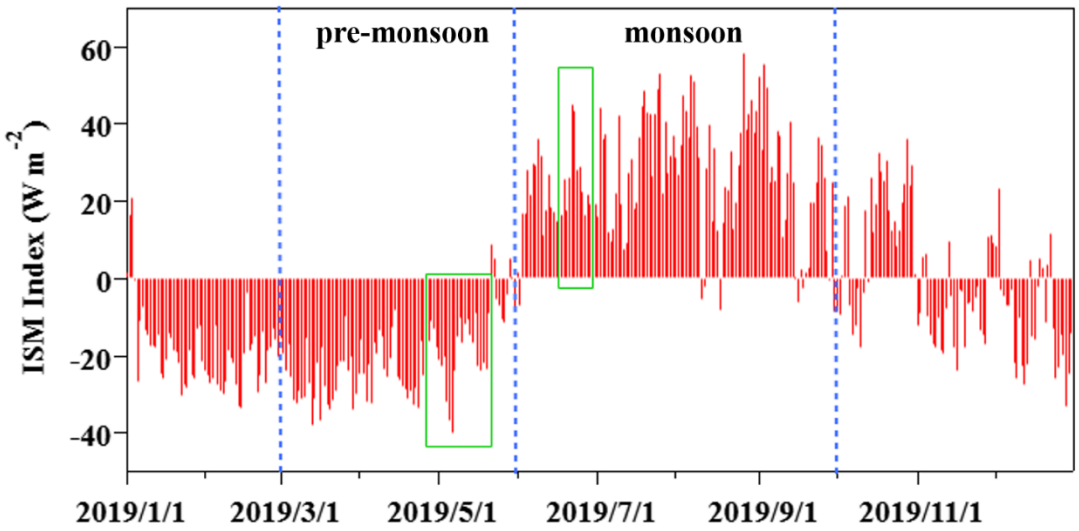

Figure S1. The Indian Summer Monsoon (ISM) Index in 2019. The measurements periods are marked by the green boxes.

Section S2 Model simulation

Model Configurations

The meteorological conditions were simulated using the Weather Research and Forecasting (WRF) (version 4.2.1) model with the FNL reanalysis dataset. The 6 h FNL data were obtained from the U.S. National Centre for Atmospheric Research (NCAR), with a spatial resolution of 1.0° × 1.0° (http://rda.ucar.edu/datasets/ds083.2/, last accessed on 28 April 2022). The physical parameterizations used in this study are the Thompson microphysical process, RRTMG longwave/shortwave radiation scheme; Noah land-surface scheme; MYJ boundary layer scheme; and modified Tiedtke cumulus parameterization scheme. The detailed configuration settings could be found in the works of Hu et al. (2016), Mao et al. (2022), Wang et al. (2021).

The Community Multiscale Air Quality version 5.3.2 (CMAQv5.3.2) model, being one of the three-dimensional chemical transport models (CTMs) (Appel et al., 2021), configured with the gas-phase mechanism of SAPRC07tic and the aerosol module of AERO6i, was employed in this study to simulate the air quality over Tibet from 24 April to 24 May and 13 June to 27 June in 2019, which contains the observation period. Air quality simulations were performed with a horizontal resolution of 12 km. The corresponding domain covered Tibet and the surrounding countries and regions with 166 × 166 grids (Fig. S2), with the 18 layers in vertical resolution. The initial and boundary conditions were provided by the default profiles. The simulated results of the first two days were not included in the model analysis, which served as a spin-up and reduced the effects of the initial conditions on the simulated results.

Model Evaluation

Previous studies have investigated the impacts of meteorological conditions on the formation, transportation, and dissipation of air pollutants (Hu et al., 2016; Hua et al., 2021; Mao et al., 2022; Sulaymon et al., 2021b; Sulaymon et al., 2021a). Therefore, the evaluation of the WRF model performance was carried out before the usage of its meteorological fields in the CMAQ simulations. The evaluation of the WRF model was achieved by comparing the predicted wind speed (WS, m/s), wind direction (WD, °) at 10 m above the surface, RH (%) and temperature (T, ℃) to the observed values. Fig. S3 showed that WS was well simulated both in pre-monsoon and monsoon seasons. WD was well simulated in pre-monsoon season, and there seems to be some deviation in the simulation of north wind in monsoon season. The main reason about the deviation in WD may be due to the poor terrain and complicated weather conditions. Nevertheless, both simulations and measurements showed more frequent southerly winds during monsoon season. RH and temperature were well simulated in the whole periods (Fig. S4). The good model performance with the statistical metrics of WS, RH and temperature meeting the suggested benchmarks are shown in Table S1. Generally, the simulated meteorological fields were qualitied and can be further utilized in driving the CMAQ model

Fig. S5 shows the comparison of simulated hourly mean concentration about PM, O_3 and VOC in observation site, which were simulated by CMAQ. The statistical indices used in evaluating the CMAQ model are present in Table S2. It can be seen

that PM and O_3 meet the suggested benchmarks, which reflect the good model performance. The observed VOC and predicted VOC in pre-monsoon season were compared to examine the model performance. The benchmarks for VOC had not been reported, but the MFB (mean fractional bias) and MFE (mean fractional error) values are within the range reported in previous VOC modelling result (Hu et al., 2017). The correlation coefficient (R) between simulated and observed VOC is 0.41, which reflected that the model can fairly simulate the variation of VOC concentration. It should be noted that VOC was underpredicted on the whole, which may due to the uncertainty of the emission inventory.

The comparison between simulated and observed SO_2 at Mt. Yulong on the southern TP is shown in Fig. S6, which helps to validate the model performance. As shown in Table S2, the statistical metrics of NMB (normalized mean bias) and NME (normalized mean error) values are within the range reported in previous SO_2 modelling result (Mao et al., 2022). The correlation coefficient (R) between simulated and observed SO_2 is 0.44, which reflected that the model can fairly simulate the variation of SO_2 concentration in Tibet.

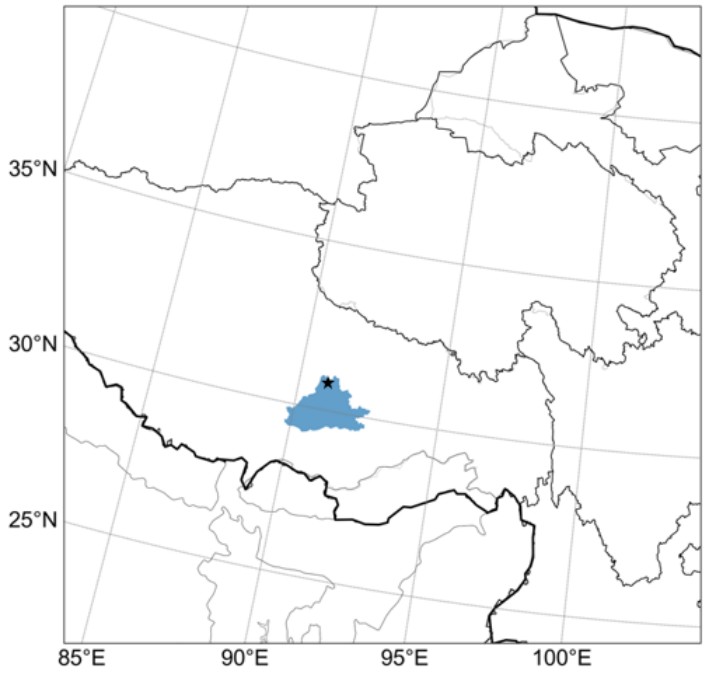

Figure S2. WRF/CMAQ modeling domain

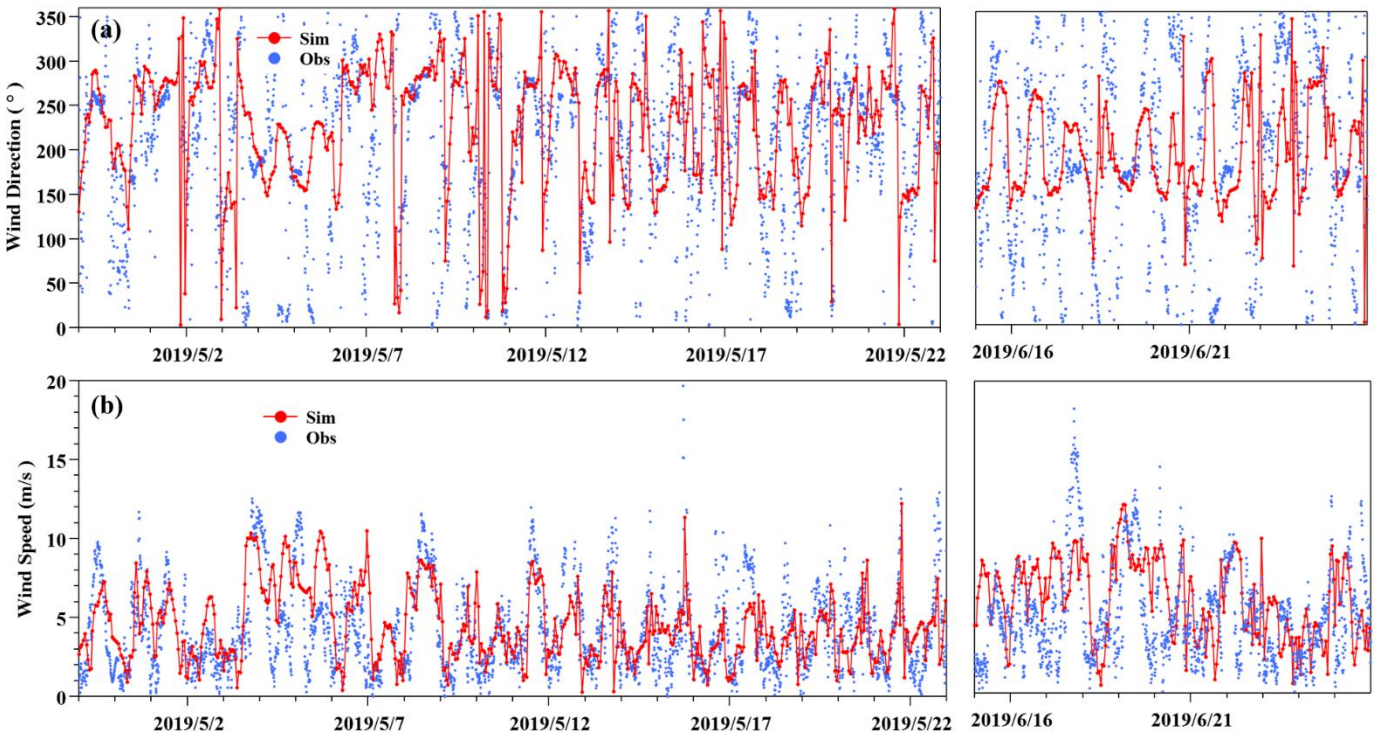

Figure S3. Comparison of simulated (in red dot-line) and observed (in blue dot) wind direction (WD, °) and wind speed (WS, m/s). Observed is 10 minutes mean data. Simulated is hourly mean data.

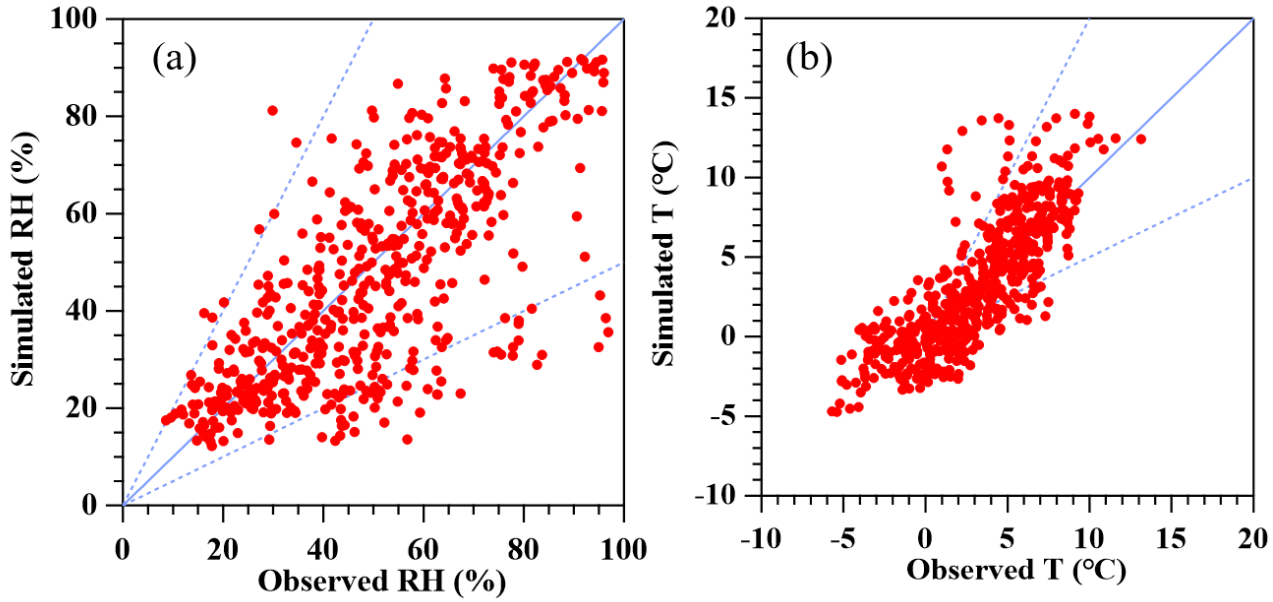

Figure S4. Comparison of simulated and observed RH (%) and temperature (T, °C). RH and temperature are hourly mean data.

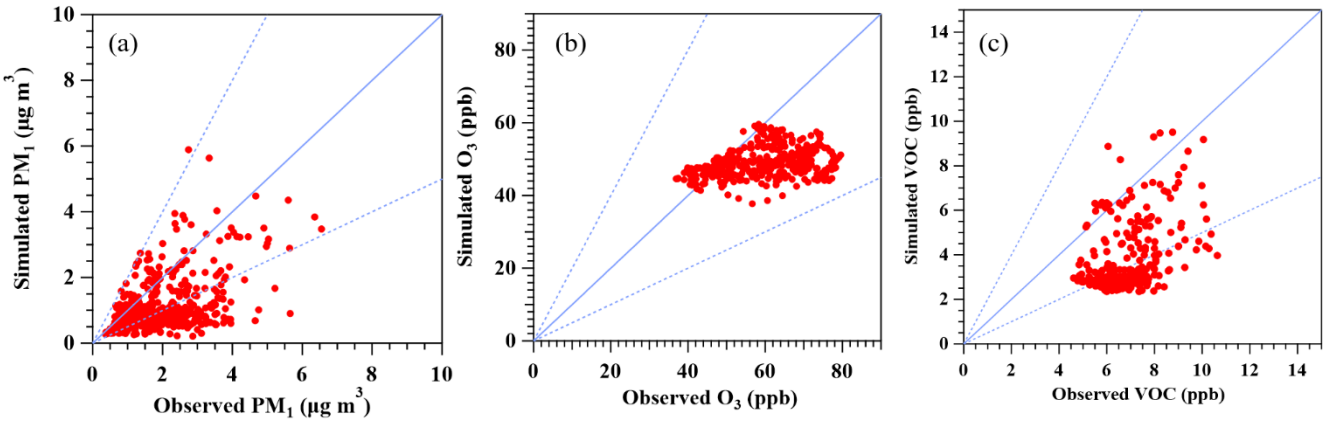

Figure S5. Comparison of simulated and observed PM (μg/m^3), O_3 (ppb) and VOC (ppb). PM, O_3 and VOC are hourly mean concentration.

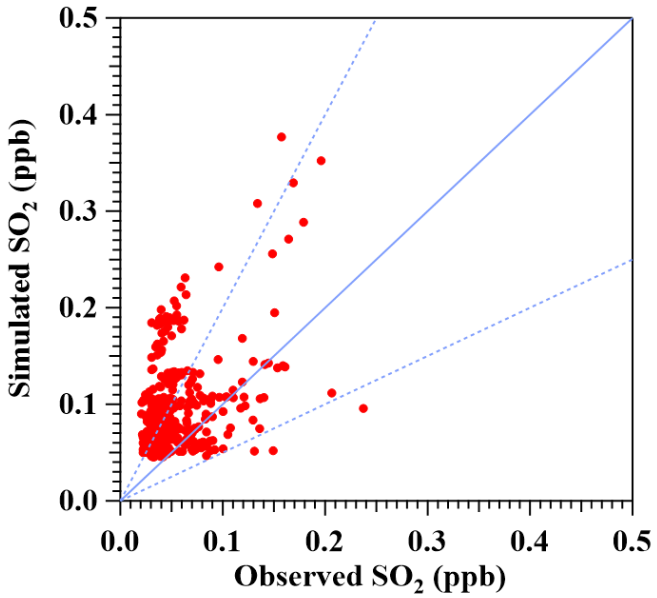

Figure S6. Comparison of simulated and observed SO_2 (ppb) at Mt. Yulong. SO_2 is hourly mean concentration.

Table S1. Model performance of meteorological factors at Nam Co station

	WS				RH				T			
	MB	**ME**	**RMSE**	**R**	**MB**	**ME**	**RMSE**	**R**	**MB**	**ME**	**RMSE**	**R**
Statistic	0.42	0.87	1.20	0.51	-1.38	12.20	16.30	0.67	0.07	1.85	2.43	0.89
Benchmarks	≤±0.5	≤2.0	≤2.0						≤±0.5	≤2.0		

MB: mean bias; ME: mean error; RMSE: root mean square error; R: correlation coefficient. The benchmarks were suggested by Boylan and Russell (2006).

Table S2. Model performance of the air pollutants at Nam Co station

	PM_1			O_3			VOC			SO_2[a]		
	MFB	**MFE**	**R**	**NMB**	**NME**	**R**	**MFB**	**MFE**	**R**	**NMB**	**NME**	**R**
Statistic	0.49	0.50	0.72	0.14	0.23	0.51	-0.47	0.49	0.41	-0.44	0.50	0.44
Benchmarks	<±0.6	<0.75	>0.4	<±0.15	<0.35	>0.5						
References							<±0.77	<0.74		<±4.38	<±4.38	0.25-0.79

NMB: normalized mean bias; NME: normalized mean error; R: correlation coefficient; MFB: mean fractional bias; MFE: mean fractional error. The benchmarks for PM and O_3 were suggested by Emery et al. (2017) and Boylan and Russell (2006), respectively. The references for VOC and SO_2 were from Hu et al. (2017) and Mao et al. (2022), respectively.

[a] The statistical metrics for evaluating SO_2 simulation at Mt. Yulong on the southern TP

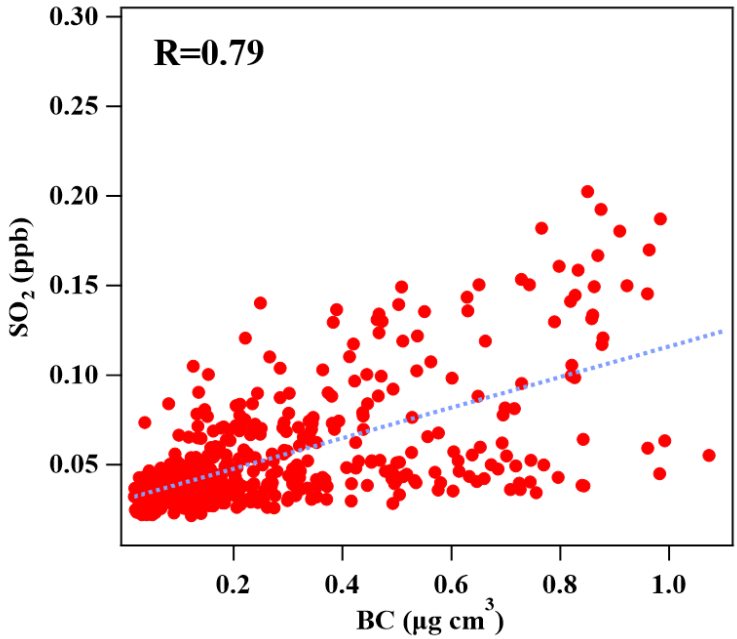

Figure S7. Relationship between SO_2 and BC at Mt. Yulong in 2015. The correlation coefficient R is 0.79.

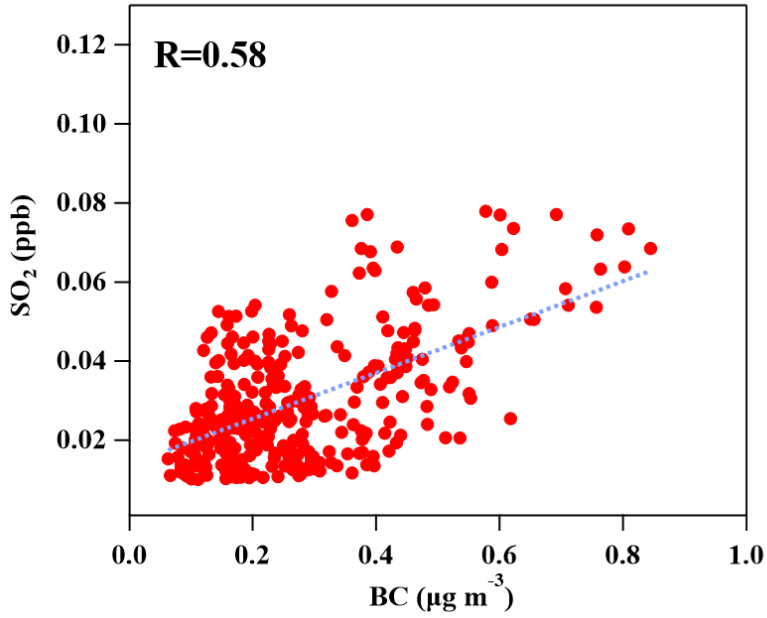

Figure S8. Relationship between modelled SO_2 and BC at Nam Co station. The correlation coefficient R is 0.58.

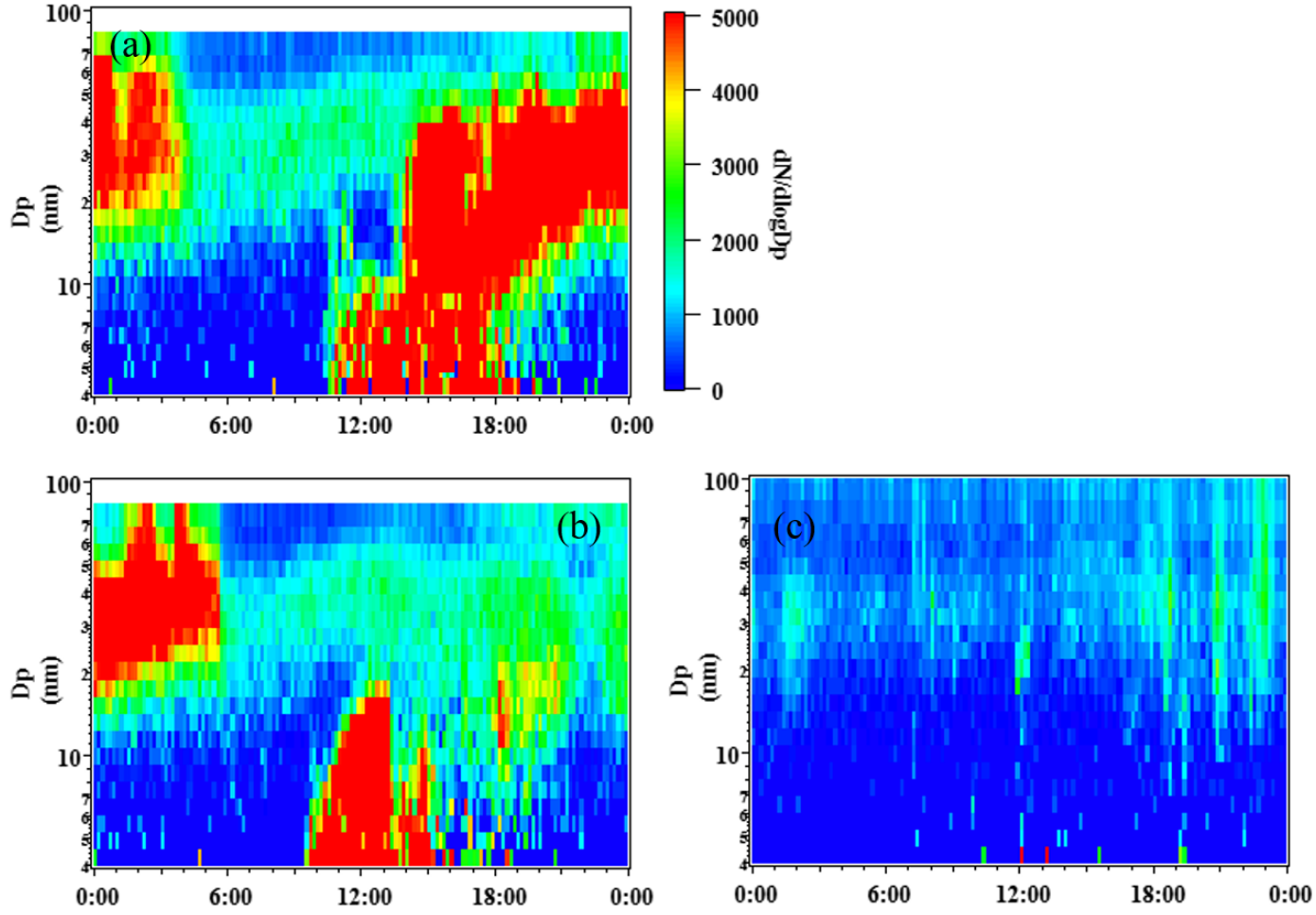

Figure S9. Typical particle number size distributions of (a) a NPF day (23 June, 2019), (b) an undefined day (24 June, 2019), and (c) a non-event day (15 May, 2019).

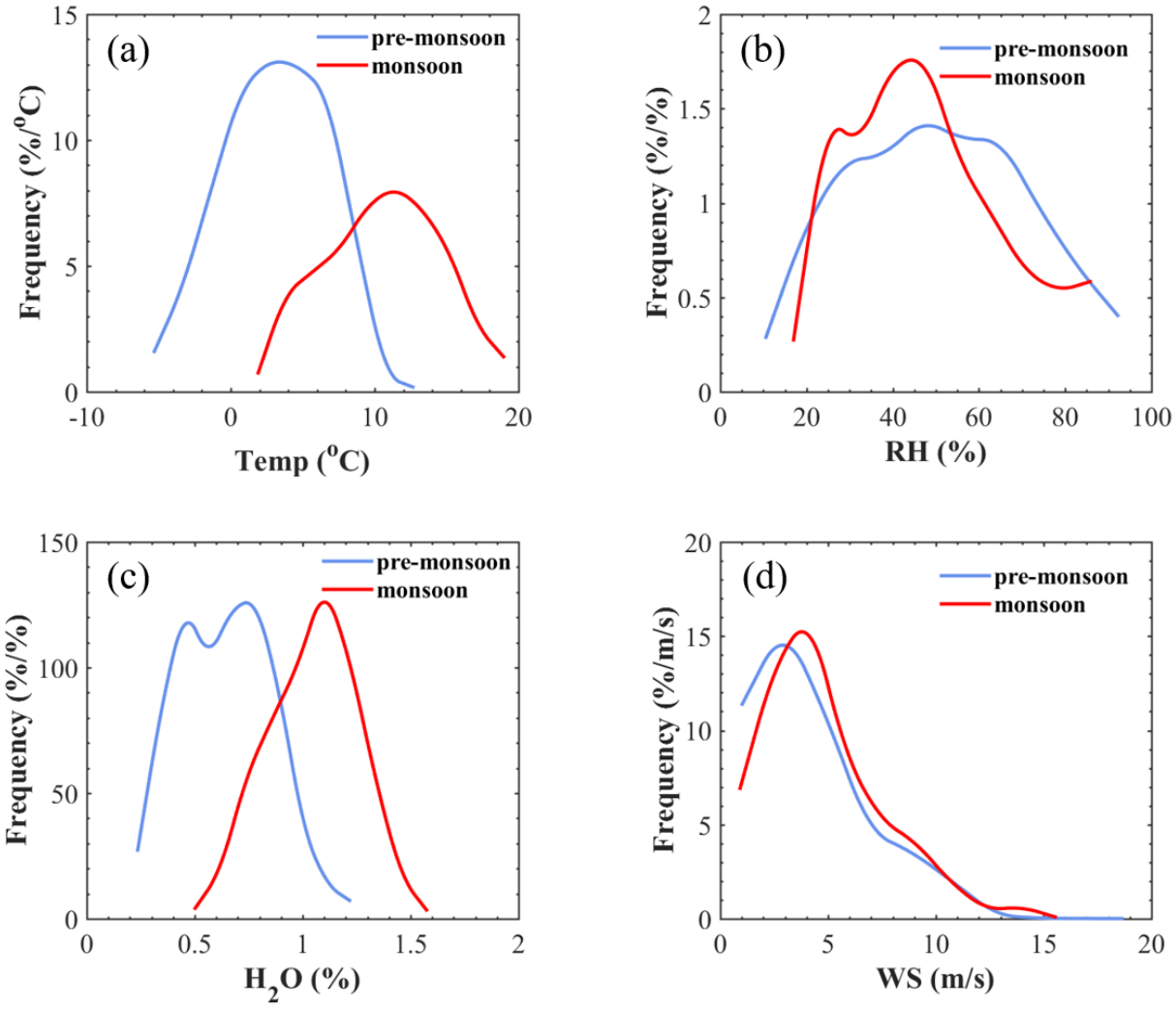

Figure S10. Comparison in frequency distributions of (a) temperature, (b) RH, (c) H_2O and (d) WS at Nam Co station in pre-monsoon and monsoon seasons.

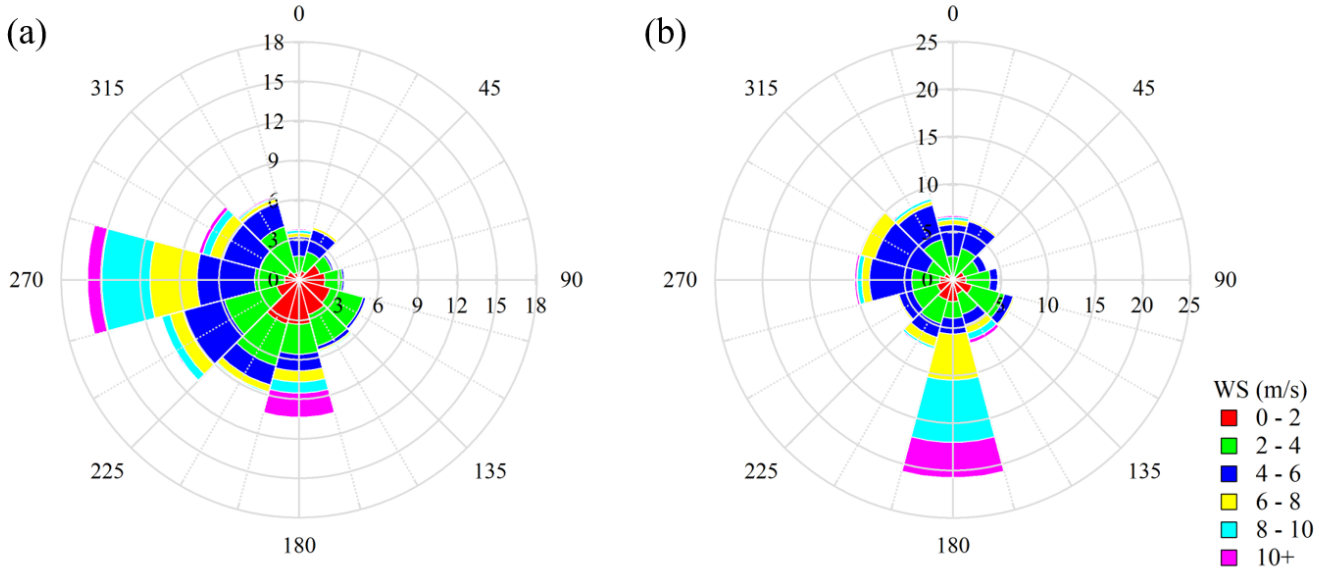

Figure S11. Wind rose plots in (a) pre-monsoon and (b) monsoon seasons. The length of each spoke on the circle represents the probability of wind coming from a particular direction at a certain range of wind speed.

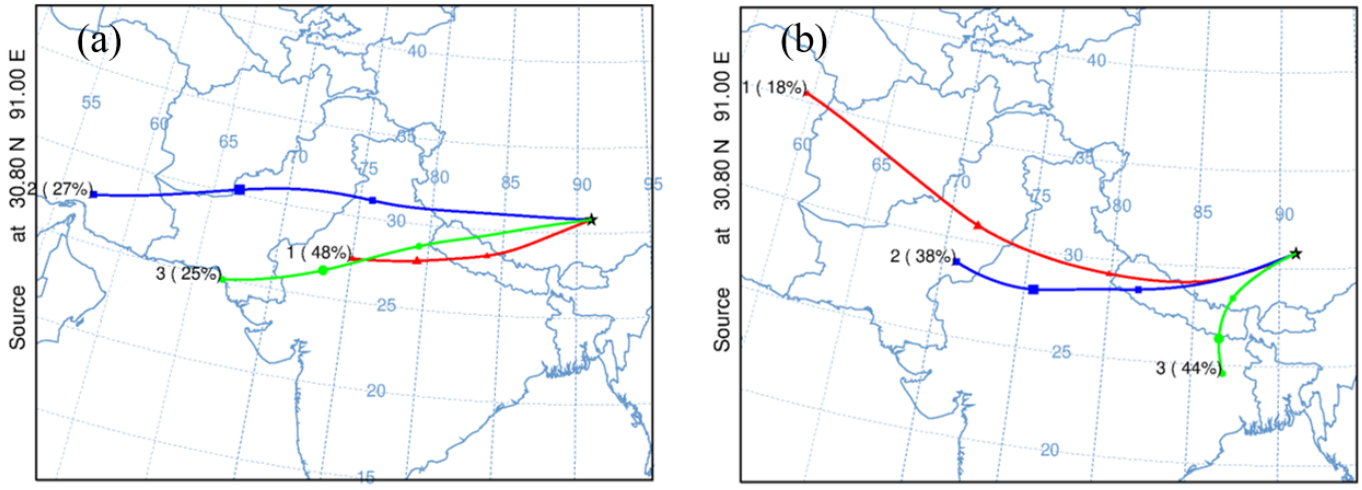

Figure S12. The frequencies of the 48 h back trajectories of air masses arriving at Nam Co station from different directions during (a) pre-monsoon and (b) monsoon seasons.

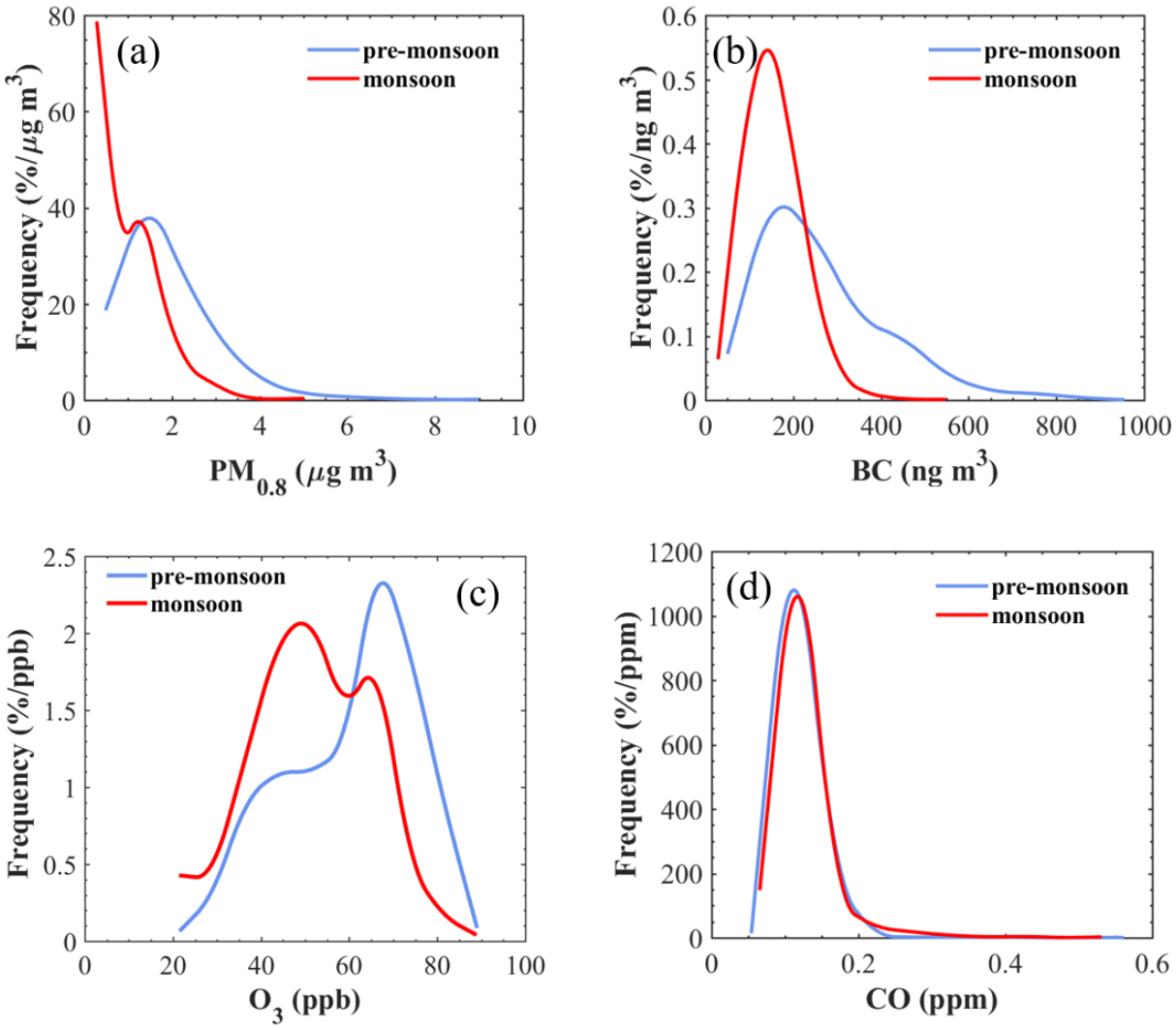

Figure S13. Comparison in frequency distributions of (a) $PM_{0.8}$, (b) BC, (c) O_3 and (d) CO at Nam Co station in pre-monsoon and monsoon seasons.

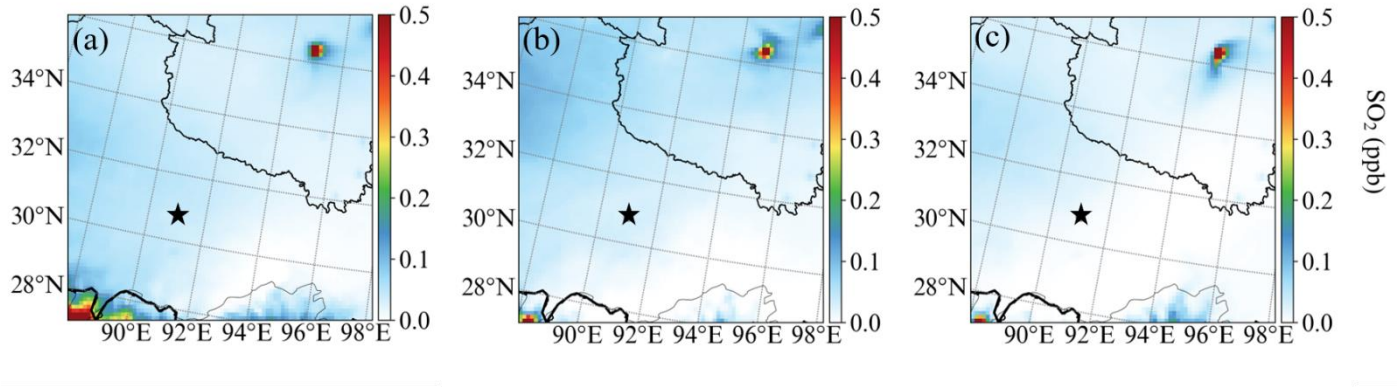

Figure S14. Model spatial distribution of SO_2 in (a) non-event days, (b) NPF-pre days, and (c) NPF-monsoon days. The star is Nam Co station.

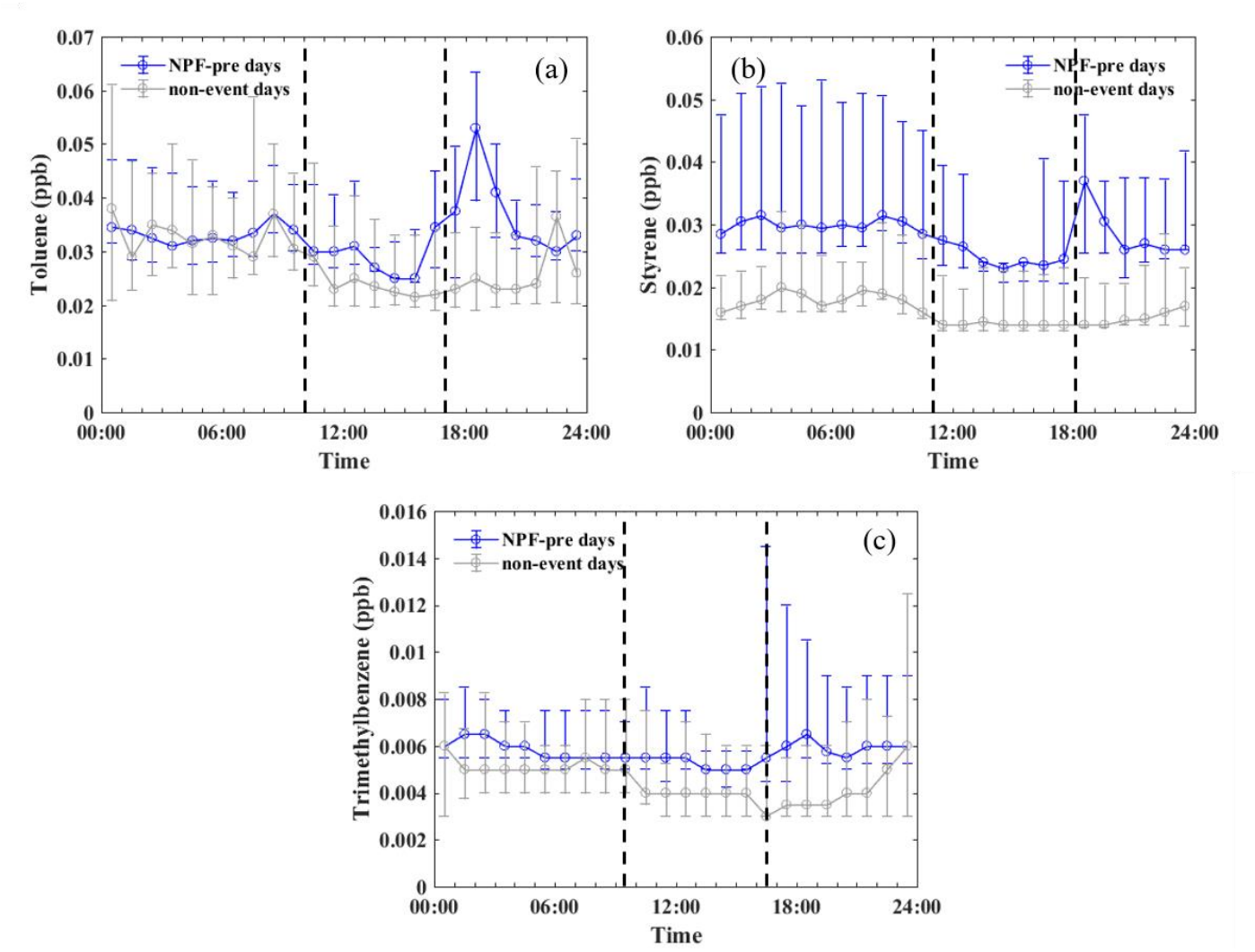

Figure S15. Diurnal variations of concentration of (a) tolunene, (b) styrene and (c) trimethylbenzene in NPF-pre days and non-event days. The upper and lower bars indicate the 75th and 25th percentiles, the markers are the average values.

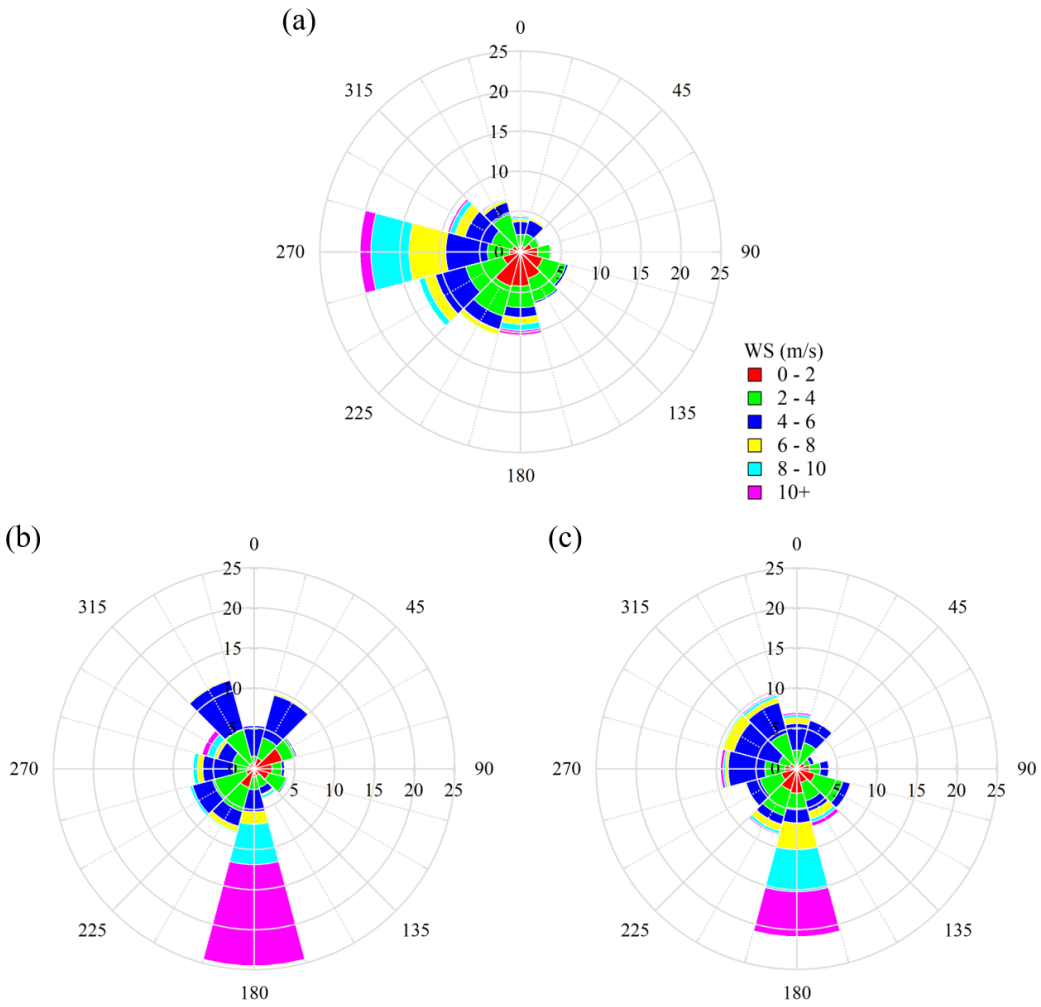

Figure S16. Wind rose plots of (a) non-event days, (b) NPF-pre days and (c) NPF-monsoon days. The length of each spoke on the circle represents the probability of wind coming from a particular direction at a certain range of wind speed.

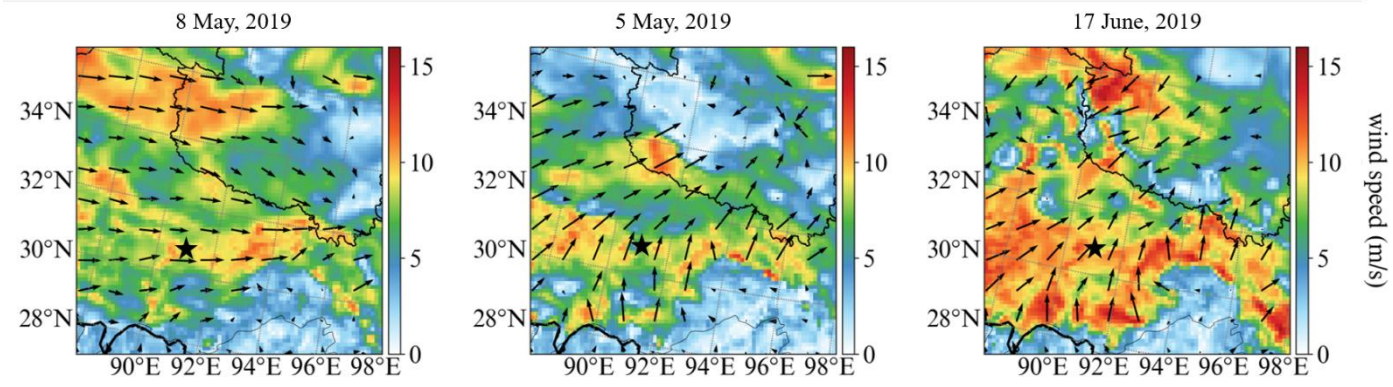

Figure S17. Model spatial distribution of wind field at 12:00 in (a) 8 May, 2019 (non-event day), (b) 5 May, 2019 (NPF-pre day), and (c) 17 June, 2019 (NPF-monsoon day), The star is Nam Co station.

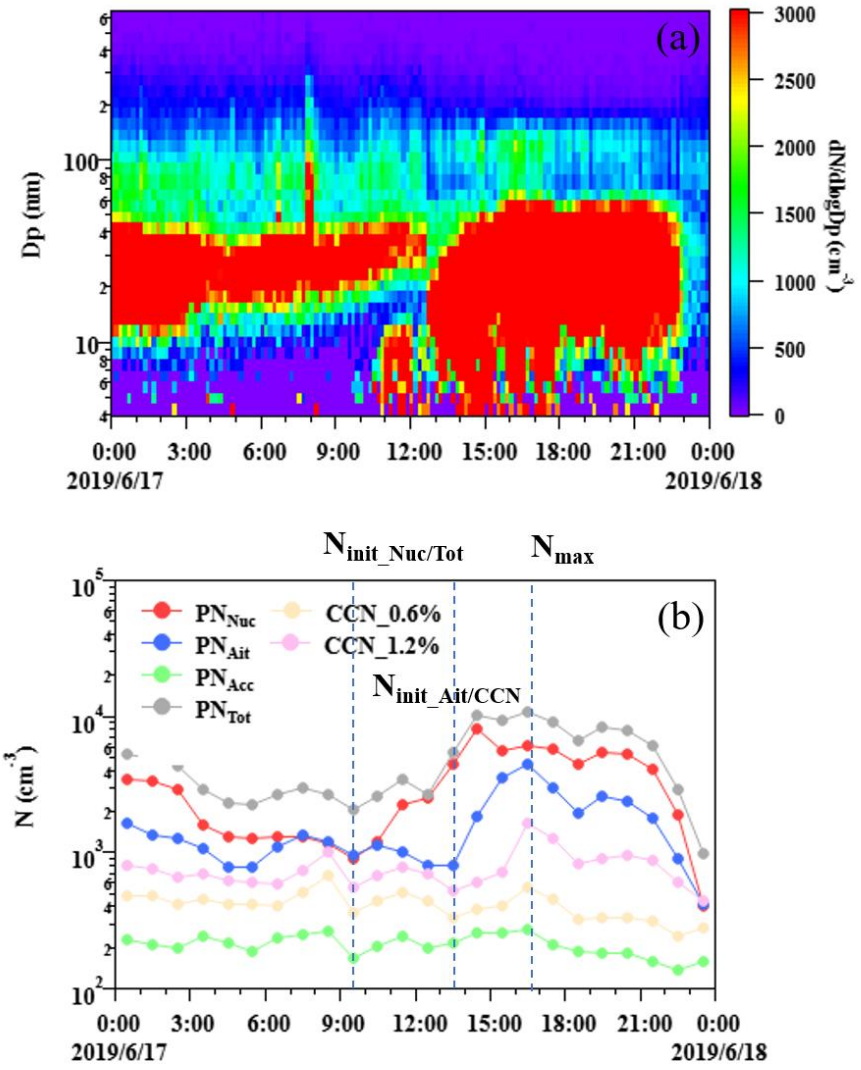

Figure S18. Determination of the aerosol production in 17 June, 2019. Time series of (a) PNSDs, and (b) the number concentrations of nucleation mode particles (PN_{Nuc}), Aitken mode particles (PN_{Ait}), accumulation mode particles (PN_{Acc}), the total particles (PN_{Tot}), CCN at S_c of 0.6% (CCN_0.6%) and 1.2% (CCN_1.2%) in 17 June, 2019. N_{init} and N_{max} denote, for each mode, the amount from which aerosol production are calculated.

References:

Appel, K. W., Bash, J. O., Fahey, K. M., Foley, K. M., Gilliam, R. C., Hogrefe, C., Hutzell, W. T., Kang, D., Mathur, R., Murphy, B. N., Napelenok, S. L., Nolte, C. G., Pleim, J. E., Pouliot, G. A., Pye, H. O. T., Ran, L., Roselle, S. J., Sarwar, G., Schwede, D. B., Sidi, F. I., Spero, T. L., and Wong, D. C.: The Community Multiscale Air Quality (CMAQ) model versions 5.3 and 5.3.1: system updates and evaluation, Geosci. Model Dev., 14, 2867-2897, 10.5194/gmd-14-2867-2021, 2021.

Bonasoni, P., Laj, P., Marinoni, A., Sprenger, M., Angelini, F., Arduini, J., Bonafè, U., Calzolari, F., Colombo, T., Decesari, S., Di Biagio, C., Di Sarra, A., Evangelisti, F., Duchi, R., Facchini, M. C., Fuzzi, S., Gobbi, G. P., Maione, M., Panday, A., Roccato, F., Sellegri, K., Venzac, H., Verza, G., Villani, P., Vuillermoz, E., and Cristofanelli, P.: Atmospheric Brown Clouds in the Himalayas: first two years of continuous observations at the Nepal Climate Observatory-Pyramid (5079 m), Atmospheric Chemistry and Physics, 10, 7515-7531, 10.5194/acp-10-7515-2010, 2010.

Boylan, J. W. and Russell, A. G.: PM and light extinction model performance metrics, goals, and criteria for three-dimensional air quality models, Atmospheric Environment, 40, 4946-4959, https://doi.org/10.1016/j.atmosenv.2005.09.087, 2006.

Cong, Z., Kang, S., Kawamura, K., Liu, B., Wan, X., Wang, Z., Gao, S., and Fu, P.: Carbonaceous aerosols on the south edge of the Tibetan Plateau: concentrations, seasonality and sources, Atmos. Chem. Phys., 15, 1573-1584, 10.5194/acp-15-1573-2015, 2015.

Emery, C., Liu, Z., Russell, A. G., Odman, M. T., Yarwood, G., and Kumar, N.: Recommendations on statistics and benchmarks to assess photochemical model performance, Journal of the Air & Waste Management Association, 67, 582-598, 10.1080/10962247.2016.1265027, 2017.

Guenther, A. B., Jiang, X., Heald, C. L., Sakulyanontvittaya, T., Duhl, T., Emmons, L. K., and Wang, X.: The Model of Emissions of Gases and Aerosols from Nature version 2.1 (MEGAN2.1): an extended and updated framework for modeling biogenic emissions, Geosci. Model Dev., 5, 1471-1492, 10.5194/gmd-5-1471-2012, 2012.

Hu, J., Chen, J., Ying, Q., and Zhang, H.: One-year simulation of ozone and particulate matter in China using WRF/CMAQ modeling system, Atmos. Chem. Phys., 16, 10333-10350, 10.5194/acp-16-10333-2016, 2016.

Hu, J., Wang, P., Ying, Q., Zhang, H., Chen, J., Ge, X., Li, X., Jiang, J., Wang, S., Zhang, J., Zhao, Y., and Zhang, Y.: Modeling biogenic and anthropogenic secondary organic aerosol in China, Atmos. Chem. Phys., 17, 77-92, 10.5194/acp-17-77-2017, 2017.

Hua, J., Zhang, Y., de Foy, B., Shang, J., Schauer, J. J., Mei, X., Sulaymon, I. D., and Han, T.: Quantitative estimation of meteorological impacts and the COVID-19 lockdown reductions on NO(2) and PM(2.5) over the Beijing area using Generalized Additive Models (GAM), Journal of environmental management, 291, 112676, 10.1016/j.jenvman.2021.112676, 2021.

Mao, J., Li, L., Li, J., Sulaymon, I. D., Xiong, K., Wang, K., Zhu, J., Chen, G., Ye, F., Zhang, N., Qin, Y., Qin, M., and Hu, J.: Evaluation of Long-Term Modeling Fine Particulate Matter and Ozone in China During 2013–2019, Frontiers in Environmental Science, 10, 10.3389/fenvs.2022.872249, 2022.

Sulaymon, I. D., Zhang, Y., Hopke, P. K., Zhang, Y., Hua, J., and Mei, X.: COVID-19 pandemic in Wuhan: Ambient air quality and the relationships between criteria air pollutants and meteorological variables before, during, and after lockdown, Atmospheric research, 250, 105362, 10.1016/j.atmosres.2020.105362, 2021a.

Sulaymon, I. D., Zhang, Y., Hopke, P. K., Hu, J., Rupakheti, D., Xie, X., Zhang, Y., Ajibade, F. O., Hua, J., and She, Y.: Influence of transboundary air pollution and meteorology on air quality in three major cities of Anhui Province, China, Journal of Cleaner Production, 329, 129641, https://doi.org/10.1016/j.jclepro.2021.129641, 2021b.

Wang, B. and Fan, Z.: Choice of South Asian Summer Monsoon Indices, Bulletin of the American Meteorological Society, 80, 629-638, 10.1175/1520-0477(1999)080<0629:COSASM>2.0.CO;2, 1999.

Wang, X., Li, L., Gong, K., Mao, J., Hu, J., Li, J., Liu, Z., Liao, H., Qiu, W., Yu, Y., Dong, H., Guo, S., Hu, M., Zeng, L., and Zhang, Y.: Modelling air quality during the EXPLORE-YRD campaign – Part I. Model performance evaluation and impacts of meteorological inputs and grid resolutions, Atmospheric Environment, 246, 118131, https://doi.org/10.1016/j.atmosenv.2020.118131, 2021.

Wiedinmyer, C., Akagi, S. K., Yokelson, R. J., Emmons, L. K., Al-Saadi, J. A., Orlando, J. J., and Soja, A. J.: The Fire INventory from NCAR (FINN): a high resolution global model to estimate the emissions from open burning, Geosci. Model Dev., 4, 625-641, 10.5194/gmd-4-625-2011, 2011.

Xu, J., Zhang, Q., Shi, J., Ge, X., Xie, C., Wang, J., Kang, S., Zhang, R., and Wang, Y.: Chemical characteristics of submicron particles at the central Tibetan Plateau: insights from aerosol mass spectrometry, Atmos. Chem. Phys., 18, 427-443, 10.5194/acp-

18-427-2018, 2018.
Yin, X., Kang, S., de Foy, B., Cong, Z., Luo, J., Zhang, L., Ma, Y., Zhang, G., Rupakheti, D., and Zhang, Q.: Surface ozone at Nam Co in the inland Tibetan Plateau: variation, synthesis comparison and regional representativeness, Atmos. Chem. Phys., 17, 11293-11311, 10.5194/acp-17-11293-2017, 2017.